Physica Scripta

PAPER

On real and complex dynamical models with hidden attractors and their synchronization

Tarek M Abed-Elhameed*, Gamal M Mahmoud and Mansour E Ahmed

Department of Mathematics, Faculty of Science, Assiut University, Assiut 71516, Egypt

* Authors to whom any correspondence should be addressed.

E-mail: tarekmalsbagh@aun.edu.eg, gmahmoud@aun.edu.eg and m_ahmed@aun.edu.eg

RECEIVED
9 January 2023

REVISED
14 February 2023

ACCEPTED FOR PUBLICATION
15 March 2023

PUBLISHED
24 March 2023

Keywords: chaotic and hyperchaotic models, fractional-order, complex model, lyapunov exponents, multi-scroll hidden attractors, combination synchronization

Abstract

In this work, we propose three chaotic (or hyperchaotic) models. These models are real or complex with one stable equilibrium point (hidden attractor). Based on a modified Sprott E model, three versions were introduced: the complex integer order, the real fractional order, and the complex fractional order. The basic properties of these models have been studied. We discover that the complex integer-order version has chaotic and hyperchaotic multi-scroll hidden attractors (MSHAs) by computing Lyapunov exponents (LEs). By making a small change to a model parameter, different MSHA values can be produced for this version. The dynamics of the real fractional version are investigated through a bifurcation diagram and LEs. It has chaotic hidden attractors for various fractional-order q values. Through varying the model parameters of the complex fractional-order (FO) version, different numbers of chaotic MSHAs can be generated. Due to the complex dynamic behaviours of the MSHAs, these models may have several applications in physics, secure communications, social relations and image encryption. A new kind of combination synchronization (CS) between one integer-order drive model and two FO response models with different dimensions is proposed. The tracking control method is used to investigate a scheme for this type of synchronization. As an example, we used our three models to test the validity of this scheme, and an agreement between the analytical and numerical results was found.

1. Introduction

Over the past few decades, a great deal of research has been done on chaotic systems in real-world models. These models appear in many important applications in neural networks, image encryption, secure communication, and physics [1–5]. Complex nonlinear dynamical models have been widely studied and investigated in the literature [6]. They have been applied in secure communication, where the doubling of the number of variables that need to be deciphered when one is using a chaotic model to transmit coded information [7]. While the complex dynamical models with fractional order have been introduced and studied, e.g. ([8, 9], and references therein). According to Shilnikov's criteria [10], there is a relation between chaotic attractors and the equilibria of their models. The existence of at least one unstable equilibrium point in dissipative dynamical models is a necessary requirement for chaos. However, in light of the discovery of hidden attractors, the conventional Shilnikov criteria have to be applied in order to confirm chaos. An attractor is referred to as a hidden attractor if its attraction basin does not overlap any small neighbourhoods of an equilibrium point; otherwise, it is referred to as a self-excited attractor [11, 12]. Both in theory and in reality, hidden attractors are extremely important. New phenomena in nonlinear dynamical models, such as the Non-Sil'nikov type of chaos, may be discovered by studying hidden attractors. In the last decade, have constructed numerous hidden chaotic model attractors ([13], and references there in).

Wang and Chen [14] presented a 3D hidden attractor of Sprott E model [15] as follows:

$$\begin{aligned}\dot{x} &= yz + a,\\ \dot{y} &= x^2 - y,\\ \dot{z} &= 1 - 4x,\end{aligned} \tag{1.0.1}$$

where x, y, and z are state variables, a is constant parameter, and dots represent time derivatives. There exist many dynamical models in various fields [16–23]. Huang and Bae [16] presented the chaotic FO love model. The chaotic FO Romeo and Juliet with an external force or external environment was studied [17]. Different cases of image encryption for chaotic dynamical systems were investigated [18–23].

Multi-scroll hidden attractors (MSHAs) have attracted extensive research interest [14, 24, 25]. So far, MSHAs topic is an open field of research. The first MSHA [26] was created by adding a nonlinear resistor with numerous breakpoints to the original Chua's circuit. The topological structures of the MSHA have been nested, and its trajectories jump on several scrolls in the phase space [24, 25]. The chaotic multi-scroll approach offers stronger security and more complex dynamic properties [27]. The MSHAs for new models are presented in [28, 29]. Piecewise linear functions are used to produce the multi-scroll attractor. Using Signum and step functions, Wang and Xiao [30] studied multi-scroll chaotic attractors. Li-Quan *et al* [31] investigated Julia fractal based on the multi-scroll memristive chaotic model. As a result, MSHAs have received increased attention in recent years.

The synchronization of models with multiple drive and response models is fascinating and significant because transmitted signals may have greater anti-translation and anti-attack capabilities. The complexity of the driving signals and their generation are equally important aspects to consider, as is communication security. Researchers looked into complex models for transmitting data signals. Recently, fractional matrix projective CS has been accomplished among complicated FO chaotic models [32]. Zerimeche *et al* [33] introduced CS of different dimensions for FO chaotic models using a scaling matrix. The modulusmodulus combination synchronization between three complex models is investigated by Mahmoud *et al* [34]. In this paper, we investigate CS using one integer-order drive model and two FO response models with different dimensions. This type of synchronization has important applications like secure communication, signal processing and safe information.

The main objectives of our paper are stated as: we propose the complex integer, real fractional and complex fractional orders versions of the model (1.0.1). The dynamics of these models, such as equilibrium points, stability, symmetry and hidden attractors are studied. By varying parameters, Yan *et al* [35] investigated different numbers of chaotic MSHAs for the real FO model. As a result, we extend the work of Ref. [35] for complex integer and fractional order models in this paper. For a small change of our parameters, we get different numbers of chaotic MSHAs for complex integer and fractional orders of the model (1.0.1). This property makes our models more secure, and it has great significance in many fields such as secure communication and image encryption. The range of the parameter a at which the complex FO form of model (1.0.1) has chaotic hidden attractors is larger than the range of the parameter a at which the complex integer-order form of model (1.0.1) has chaotic hidden attractors. A new type of combination synchronization (CS) is introduced. A scheme to achieve this new type of CS is presented.

This paper is organized as follows. Section 2 proposes the complex integer-order version of model (1.0.1). We investigate its dynamics and different numbers of chaotic and hyperchaotic MSHAs by varying the parameter a. The FO form of model (1.0.1) is given in section 3. The bifurcation diagram is plotted for this model. In section 4, we introduce the FO form of the model of section 2. This version has a wider range of chaotic attractors than the integer version. Section 5 contains the combination synchronization and its scheme to achieve it. There is good agreement between the numerical and analytical calculations. Section 6 contains our paper's conclusion and future work.

2. Basic properties of the complex form of model (1.0.1)

In this section we introduce the complex form of model (1.0.1) which is:

$$\begin{aligned}\dot{x} &= yz + a,\\ \dot{y} &= x^2 - y,\\ \dot{z} &= 1 - 2(x + \bar{x}),\end{aligned} \tag{2.0.1}$$

where $x = u_1 + iu_2$ and $y = u_3 + iu_4$ are complex variables, $z = u_5$ is real variable, $i = \sqrt{-1}$ and $\bar{x}$ denotes complex conjugate of x, $a > 0$. The real version of model (2.0.1) reads:

$$\begin{aligned}\dot{u_1} &= u_3u_5 + a,\\ \dot{u_2} &= u_4u_5,\\ \dot{u_3} &= u_1^2 - u_2^2 - u_3,\\ \dot{u_4} &= 2u_1u_2 - u_4,\\ \dot{u_5} &= 1 - 4u_1.\end{aligned} \tag{2.0.2}$$

2.1. Lyapunov exponents and Lyapunov dimension

Since (2.0.2) is a 5-D model, it has a five LEs $\mu_r, r = 1, 2, ..., 5$, which may calculated as follows: model (2.0.2) in matrix form is:

$$\dot{U}(t) = f(U(t); \xi), \tag{2.1.1}$$

where, $U(t) = (u_1(t), u_2(t), u_3(t), u_4(t), u_5(t))^T$ is the solution we wish to determine, $f = (f_1, f_2, f_3, f_4, f_5)^T$, ξ is a set of parameters and T denotes transpose. The equations governing small deviations δU about the trajectory $U(t)$ are

$$\delta\dot{U}(t) = M_{r,j}(U(t); \xi)\delta U, \qquad r, j = 1, 2, ..., 5, \tag{2.1.2}$$

where, $M_{r,j} = \frac{\partial f_r}{\partial u_j}$ is the Jacobian matrix:

$$M_{r,j} = \begin{pmatrix} 0 & 0 & u_5 & 0 & u_3\\ 0 & 0 & 0 & u_5 & u_4\\ 2u_1 & -2u_2 & -1 & 0 & 0\\ 2u_2 & 2u_1 & 0 & -1 & 0\\ -4 & 0 & 0 & 0 & 0 \end{pmatrix}. \tag{2.1.3}$$

The LEs of a dynamical model are given in [36, 37]. Numerically all the LEs values are computed by Wolf algorithm [38].

$$\mu_r = \lim_{t\to 0}\frac{1}{t}\ln\frac{\|\delta u_r(t)\|}{\|\delta u_r(0)\|}, \tag{2.1.4}$$

where $\delta u_r(0)$, $\delta u_r(t)$ are deviation vectors from the given orbit, at times $t = 0$ and $t > 0$, respectively.

The Lyapunov dimension of the solution of model (2.0.2) is defined according to Kaplan-Yorke conjecture as [39]:

$$D = M + \frac{\sum_{k=1}^{M}\mu_k}{|\mu_{M+1}|}, \tag{2.1.5}$$

where M is the largest integer s.t. $\sum_{k=1}^{M}\mu_k > 0$ and $\sum_{k=1}^{M+1}\mu_k < 0$.

2.2. Dynamics of model (2.0.2)

Model (2.0.2) is symmetric about the coordinates u_2, u_4 and dissipative for all values of parameter a since $\nabla.f = \frac{\partial\dot{u_1}}{\partial u_1} + \frac{\partial\dot{u_2}}{\partial u_2} + ... + \frac{\partial\dot{u_5}}{\partial u_5} = -2 < 0$. This model has one equilibrium point $E_0 = \left(\frac{1}{4}, 0, \frac{1}{16}, 0, -16a\right)^T$. The Jacobian matrix of model (2.0.2) at E_0 is:

$$J_{E_0} = \begin{pmatrix} 0 & 0 & -16a & 0 & 1/16\\ 0 & 0 & 0 & -16a & 0\\ \frac{1}{2} & 0 & -1 & 0 & 0\\ 0 & \frac{1}{2} & 0 & -1 & 0\\ -4 & 0 & 0 & 0 & 0 \end{pmatrix}. \tag{2.2.1}$$

The characteristic equation of J_{E_0} is written as:

$$f(\lambda) = \lambda^5 + 2\lambda^4 + (16a + 1.25)\lambda^3 + (16a + 0.5)\lambda^2 + (64a^2 + 2a + 0.25)\lambda + 2a. \tag{2.2.2}$$

From RouthHurwitz stability criterion, it is clear that if $a > 0$, then E_0 is stable. For the choice $a = 0.03$, then the corresponding eigenvalues of E_0 are $\lambda_1 = -0.782174$, $\lambda_2 = -0.6$, $\lambda_3 = -0.4$, and $\lambda_{4,5} = -0.108913 \pm 0.554761i$.

2.3. Multi-scroll chaotic and hyperchaotic hidden attractors for model (2.0.2)

In this subsection we discuss the effect of parameter a in model (2.0.2) to get different chaotic and hyperchaotic MSHAs. The LEs (2.1.4) for model (2.0.2) for the initial conditions $u_0 = (2{,}1,\ 3{,}2{,}9)^T$ and $a \in [0, 0.15]$ are

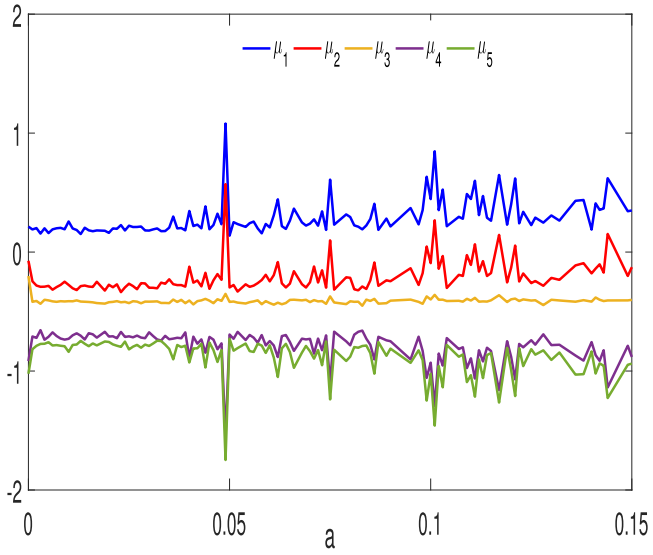

Figure 1. The LEs versus $a \in [0, 0.15]$ for model (2.0.2).

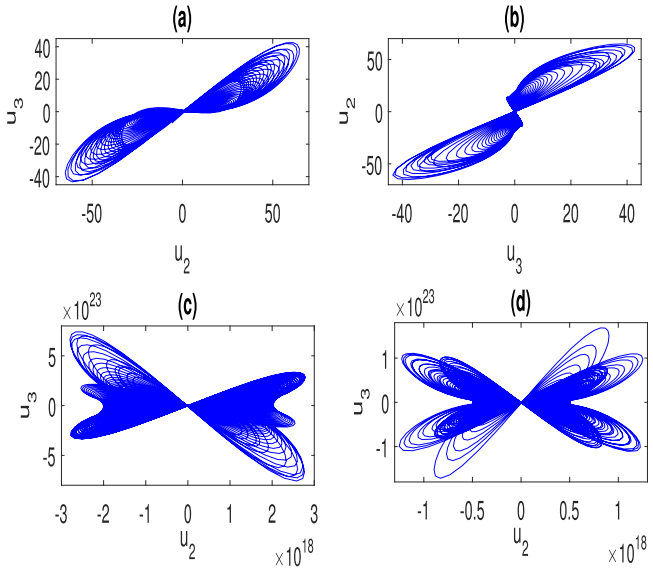

Figure 2. Chaotic MSHAs (2, 4, 6 and 10) for model (2.0.2): (a) 2-scroll hidden attractors with $a = 0.0364$, (b) 4-scroll hidden attractors with $a = 0.03644$, (c) 6-scroll hidden attractors with $a = 0.0988$, and (d) 10-scroll hidden attractors with $a = 0.037$.

computed. Model (2.0.2) has hyperchaotic MSHAs for $a = 0.049, 0.075, 0.099, 0.101, 0.111, 0.117$, and 0.144, while it has chaotic MSHAs for the remain values of parameters $a \in [0, 0.15]$ as shown in figure 1. If we choose different positive values of a and the same initial conditions in figure 1, the MSHAs are plotted in figure 2 in (u_2, u_3) space. Figure 2(a) shows chaotic 2-scroll hidden attractors for $a = 0.0364$, while 4-scroll hidden attractors for this model is shown figure 2(b) when $a = 0.03644$. In figure 2(c), 6-scroll hidden attractors is depicted for $a = 0.0988$ and 10-scroll hidden attractors when $a = 0.037$ is given in figure 2 (d). For the choice $a = 0.049$ for model (2.0.2), the corresponding LEs are: $\mu_1 = 1.0802$, $\mu_2 = 0.5712$, $\mu_3 = -0.3512$, $\mu_4 = -1.5509$, and $\mu_5 = -1.7478$ and the Lyapunov dimension (2.1.5) is $D = 3.8384$. Figure 3 contains the hyperchaotic MSHAs (6-scroll) for $a = 0.049$.

Remark 2.1. We noticed that the complex form of model (1.0.1) has rich dynamics than the real one, different chaotic and hyperchaotic MSHAs are appeared only in complex model (2.0.1). The range of the parameter a of chaotic MSHAs for model (2.0.1) is bigger than the one of real form (1.0.1) [14].

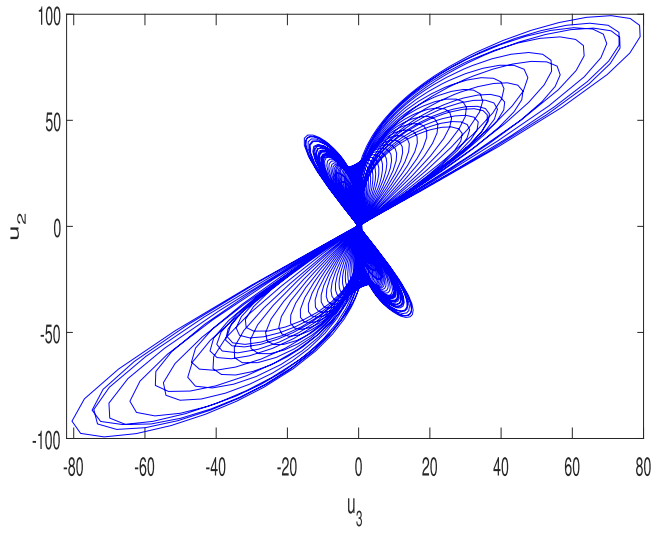

Figure 3. Hyperchaotic 6-scroll hidden attractors for model (2.0.2) for $a = 0.049$.

Remark 2.2. The complex model (2.0.1) has chaotic and hyperchaotic MSHAs, while model (1.0.1) has only chaotic ones. The security of the sent communications may improve with more model variables.

3. The FO version of model (1.0.1)

The FO form of model (1.0.1) is:

$$\begin{aligned} {}^{c}D^{q}x &= yz + a,\\ {}^{c}D^{q}y &= x^{2} - y,\\ {}^{c}D^{q}z &= 1 - 4x, \end{aligned} \tag{3.0.1}$$

where ${}^{c}D^{q}$ is the Caputo fractional derivatives [40]. Model (3.0.1) is not symmetric, but it is dissipative for all values of a. This model has only one equilibrium point $E_1 = \left(\frac{1}{4}, \frac{1}{16}, -16a\right)^{T}$. The corresponding characteristic polynomial of E_1 is:

$$f(\lambda) = \lambda^{3} + \lambda^{2} + (8a + 0.25)\lambda + 0.25. \tag{3.0.2}$$

The equilibrium point E_1 is stable if $|arg(\lambda_k)| > \frac{q\pi}{2}, k = 1, 2, 3$. For example if $a > 0$, then E_1 is stable.

Using AdamBashforthMoluton method [41], the results of model (3.0.1) are stated. The chaotic attractor for this model for $q = 0.99$ and $a = 0.003$ is appeared in figures 4(a)–(b) in 3 and 2-spaces, respectively although it has only one stable equilibrium point. The bifurcation diagram for model (3.0.1) with $q = 0.99$ for $a \in [0, 0.047]$ is plotted in figure 4(c). Figure 4(d) shows the largest Lyapunov exponent (the maximum value of (2.1.4)) for model (3.0.1) versus $q \in [0.9, 1]$.

Remark 3.1. The security in the fractional model (3.0.1) is complicated than the integer model (1.0.1) because it has the fractional parameter q beside the parameter a. Increasing the model parameters increased the security of the transmitted signals [7].

4. The complex FO of model (1.0.1)

The FO version of model (2.0.2) can be written as:

$$\begin{aligned} {}^{c}D^{q}u_1 &= u_3u_5 + a,\\ {}^{c}D^{q}u_2 &= u_4u_5,\\ {}^{c}D^{q}u_3 &= u_1^{2} - u_2^{2} - u_3,\\ {}^{c}D^{q}u_4 &= 2u_1u_2 - u_4,\\ {}^{c}D^{q}u_5 &= 1 - 4u_1. \end{aligned} \tag{4.0.1}$$

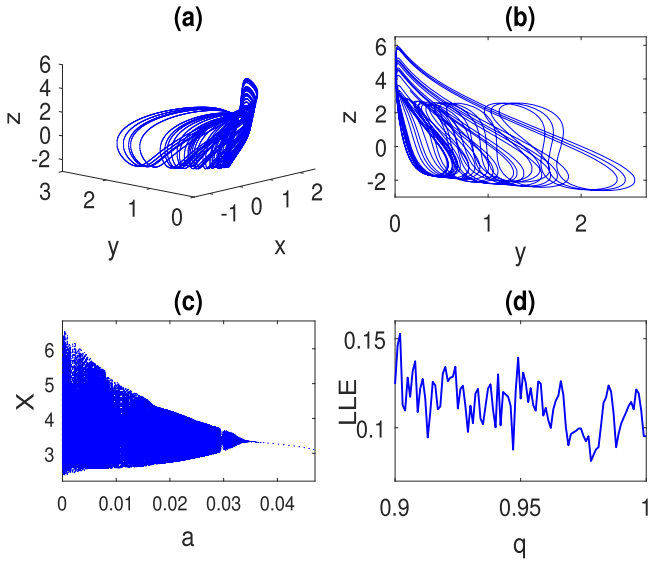

Figure 4. For model (3.0.1): (a) the chaotic attractor for $q = 0.99$ and $a = 0.003$ in (x, y, z) space, (b) in (y, z) space, (c) the bifurcation diagram for $a \in [0, 0.047]$, (d) the largest Lyapunov exponent versus $q \in [0.9, 1]$.

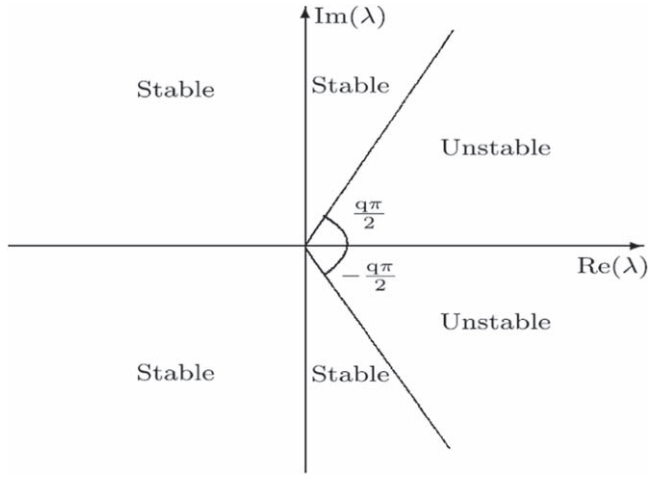

Figure 5. Stability region of a FO model with order $0 < q < 1$.

The dynamics of model (4.0.1) is the same as of the model (2.0.2) except the stability condition which is $|arg(\lambda_r)| > \frac{q\pi}{2}, r = 1, 2,...,5$. This condition makes the region of stability in FO dynamical model is larger than integer version as shown in figure 5.

In numerical simulation, the LEs for model (4.0.1) are plotted in figure 6. Figure 6(a) shows the LEs versus $q \in [0.99, 1]$, while the LEs versus $a \in [0, 10]$ are presented in figure 6(b). Chaotic MSHAs with 4, 6, 8 and 10 scrolls for model (4.0.1) with $a = 32$ and the initial conditions $u_0 = (1{,}2,\ 3{,}4{,}5)^T$ are depicted in figures 7(a)–(d) for $q = 0.992, 0.9943, 0.995, 0.99517$, respectively. For another value of $q = 0.99516$, 16-scroll hidden attractors is found and it is shown in figure 8.

By fixing $q = 0.995$ and varying the parameter a with the same initial conditions as in figure 8 for model (4.0.1), we get MSHAs with 2, 4, 6, and 8 scrolls as shown in figure 9.

Remark 4.1. It is noted that by choosing appropriate values of the model parameters q and a, one can obtain different numbers of chaotic MSHAs.

Remark 4.2. It is clear that from figure 1 and figure 6(b) the region of parameter a at which model (4.0.1) has chaotic MSHAs is larger than one for model (2.0.2).

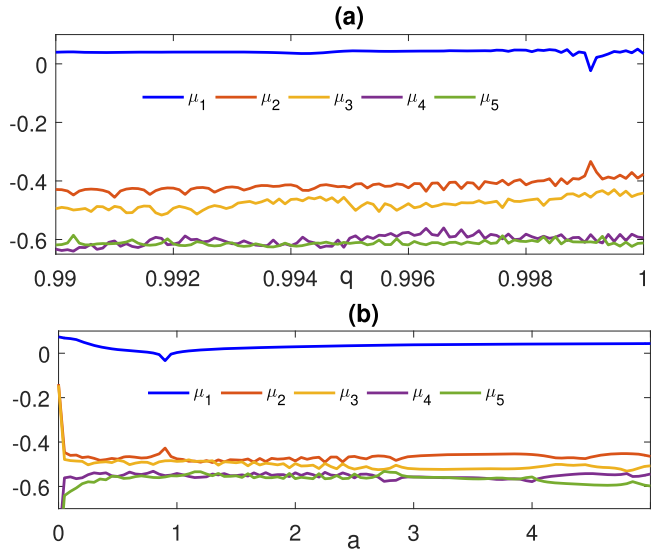

Figure 6. The LEs for model (4.0.1) versus: (a) $q \in [0.99, 1]$, (b) $a \in [0, 10]$.

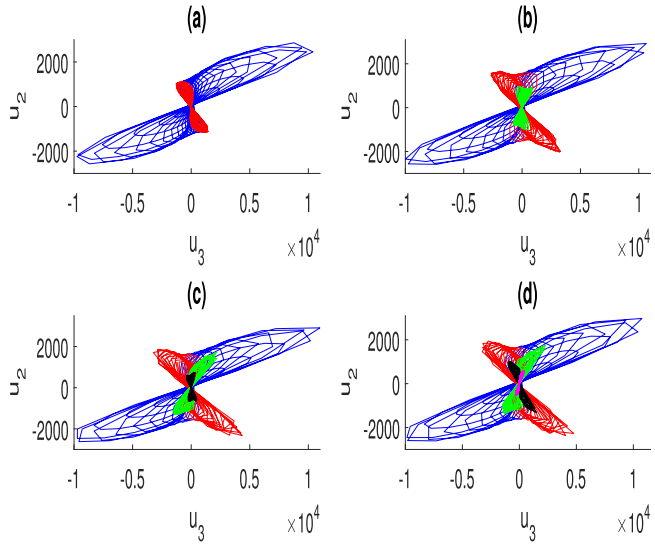

Figure 7. Chaotic MSHAs with 4, 6, 8 and 10 scrolls for model (4.0.1) with $a = 32$ by setting different values of aq: (a) $q = 0.992$, (b) $q = 0.9943$, (c) $aq = 0.995$, and (d) $q = 0.99517$.

Remark 4.3. Model (2.0.2) has hyperchaotic attractors while its FO version (4.0.1) does not.

Remark 4.4. Our model (4.0.1) has a chaotic 16-scroll hidden attractor, while the model (2.0.2) does not have it.

Remark 4.5. The MSHAs appeared only for model (2.0.2) and (4.0.1).

5. Combination synchronization (CS) between one integer-order and two FO models with different dimensions

Based on the tracking control method [42], the CS between one integer-order and two FO models with different dimensions is presented. The one integer-order and two FO models can be written, respectively, as:

$$\dot{u} = f(u(t)), \qquad u \in \mathbf{R^n}, \tag{5.0.1}$$

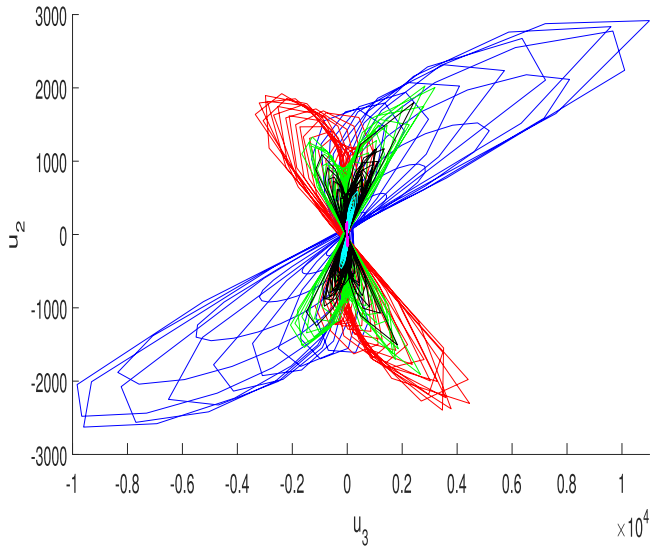

Figure 8. 16-scroll hidden attractors for model (4.0.1) for $a = 32$ and $q = 0.99516$.

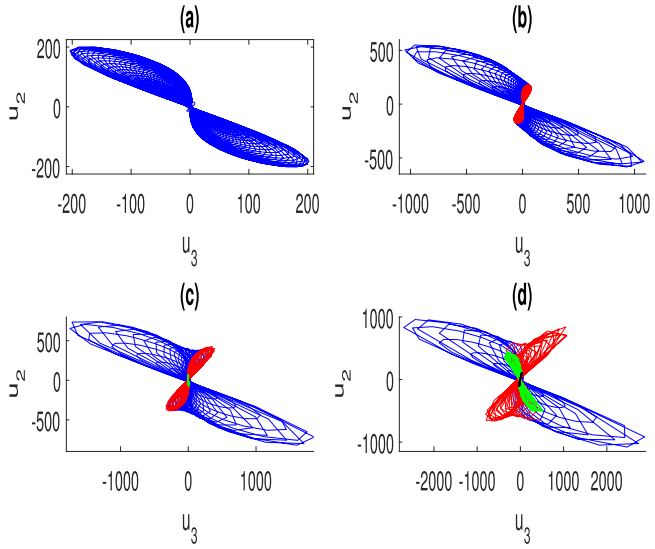

Figure 9. Chaotic MSHAs with 2, 4, 6, and 8 scrolls for model (4.0.1) with $q = 0.995$ for different values of a: (a) $a = 6.6$, (b) $a = 5$, (c) $a = 4.3$, and (d) $a = 3.8$.

$$
\begin{aligned}
{}^{c}D^{q}v &= g(v(t)) + \eta, \qquad v, \eta \in \mathbf{R}^{m}, \\
{}^{c}D^{q}w &= h(w(t)) + \zeta, \qquad w, \zeta \in \mathbf{R}^{l},
\end{aligned} \tag{5.0.2}
$$

where, $u = (u_1, u_2, ..., u_n)^T$, $v = (v_1, v_2, ..., v_m)^T$ and $w = (w_1, w_2, ..., w_l)^T$ are the state vectors of models (5.0.1)–(5.0.2), $\eta = (\eta_1, \eta_2, ..., \eta_m)^T$, $\zeta = (\zeta_1, \zeta_2, ..., \zeta_l)^T$, are the vector of control functions which is a function of u, v, w and T denotes the transpose.

Definition 5.1. The CS between the one integer-order drive model (5.0.1) and the two FO response models (5.0.2) with different dimensions can be achieved if:

$$
\lim_{t\to\infty} \|e\| = \lim_{t\to\infty} \|M_1 v + M_2 w - M_3 u\| = 0, \tag{5.0.3}
$$

where, the constant matrices $M_1 \in \mathbf{R}^n \times \mathbf{R}^m$, $M_2 \in \mathbf{R}^n \times \mathbf{R}^l$, $M_3 \in \mathbf{R}^n \times \mathbf{R}^n$, $\|\cdot\|$ is the matrix norm and $e \in \mathbf{R}^n$ is the synchronization error.

Remark 5.1. If $n = m = l$ and $q = 1$ in the two response models (5.0.2), we obtain the CS for models that share the same dimension as those that have been researched in the literature [43, 44].

Remark 5.2. If $q = 1$ in the two response models (5.0.2), we get the CS between three integer-order models with the different dimension [45].

Remark 5.3. If $n = m$ in the models (5.0.1)–(5.0.2), M_1, M_2 are $(n \times n)$ identity matrices and $w = 0$ in the error model (5.1), we get the complete synchronization between the integer-order and FO models [46].From the response models (5.0.2), one can get

$$M_1\,{}^cD^q v + M_2\,{}^cD^q w = M_1 g(v(t)) + M_2 h(w(t)) + U, \tag{5.0.4}$$

where $U = M_1\eta + M_2\zeta = \rho(u) + \tau(u, v, w)$ is the control functions, τ: $\mathbf{R}^n \times \mathbf{R}^m \times \mathbf{R}^l \longrightarrow \mathbf{R}^n$ is a vector function, and later it will be define, and $\rho(u) \in \mathbf{R}^n$ is a compensation control given by:

$$\rho(u) = M_3\,{}^cD^q u - f(M_3 u). \tag{5.0.5}$$

Using equations (5.0.4)–(5.0.5), the error model between the integer-order derive model (5.0.1) and the FO response models (5.0.2) can be obtained as follows:

$${}^cD^q e = M_1 g(v) + M_2 h(w) - f(M_3 u) + \tau(u, v, w). \tag{5.0.6}$$

If the model of error (5.0.6) is asymptotically stable, the CS between the drive model (5.0.1) and the response models (5.0.2) can be hold. To construct the analytical formula for the vector function $\tau(u, v, w)$ for which the error model (5.0.6) is asymptotically stable, the following theorem is introduced.

Theorem 5.1. *CS of one integer-order drive model (5.0.1) and two FO response models (5.0.2) will be achieved if the control functions $\tau(u, v, w)$ are designed as follows:*

$$\tau(u, v, w) = f(M_3 u) - M_1 g(v) - M_2 h(w) - Ke, \tag{5.0.7}$$

where, $K \in \mathbf{R}^n \times \mathbf{R}^n$ is the control gain matrix.

Proof. Let the Lyapunov function be $V(e(t)) = 1/2e^T(t)e(t)$, then

$${}^cD^q V(e(t)) = {}^cD^q\{1/2e^T(t)e(t)\}. \tag{5.0.8}$$

According to remark 1 in [47], we have

$${}^cD^q V(e(t)) \leqslant e^T(t)\,{}^cD^q e(t). \tag{5.0.9}$$

It follows from equations (5.0.6), (5.0.7) and (5.0.9) that

$$\begin{aligned} {}^cD^q V(e(t)) &\leqslant -Ke^T(t)e(t) \\ &\leqslant -\lambda_{\min} e^T(t)e(t), \end{aligned} \tag{5.0.10}$$

where $\lambda_{\min}$ is the minimum eigenvalue of K. Then it follows from theorem 1 [47] that $\lim_{t\to\infty} \|e(t)\| = 0$. □

5.1. An example

An illustration is provided in this subsection to demonstrate the validity of the analytical results of our theorem 5.1. We assume the 5D integer-order model (2.0.2) is the drive model and the 3D FO model (3.0.1) and 5D FO model (4.0.1) are the response models. The 3D and 5D response models can be written after adding the control functions, respectively, as:

$$\begin{aligned} {}^cD^q v_1 &= v_2 v_3 + a + \eta_1, \\ {}^cD^q v_2 &= v_1^2 - v_2 + \eta_2, \\ {}^cD^q v_3 &= 1 - 4v_1 + \eta_3, \end{aligned} \tag{5.1.1}$$

and

$$\begin{aligned} {}^cD^q w_1 &= w_3 w_5 + a + \zeta_1, \\ {}^cD^q w_2 &= w_4 w_5 + \zeta_2, \\ {}^cD^q w_3 &= w_1^2 - w_2^2 - w_3 + \zeta_3, \\ {}^cD^q w_4 &= 2w_1 w_2 - w_4 + \zeta_4, \\ {}^cD^q w_5 &= 1 - 4w_1 + \zeta_5, \end{aligned} \tag{5.1.2}$$

where $U = M_1\eta + M_2\zeta = \rho(u) + \tau(u, v, w)$ is the control functions, $U = (U_1, U_2, U_3, U_4, U_5)^T$, $\eta = (\eta_1, \eta_2, \eta_3)^T$, $\zeta = (\zeta_1, \zeta_2, \zeta_3, \zeta_4, \zeta_5)^T$, $M_1 \in \mathbf{R}^{5\times 3}$, $M_2 \in \mathbf{R}^{5\times 5}$ are two constant matrices, and $\rho(u)$, $\tau(u, v, w) \in \mathbf{R}^5$.

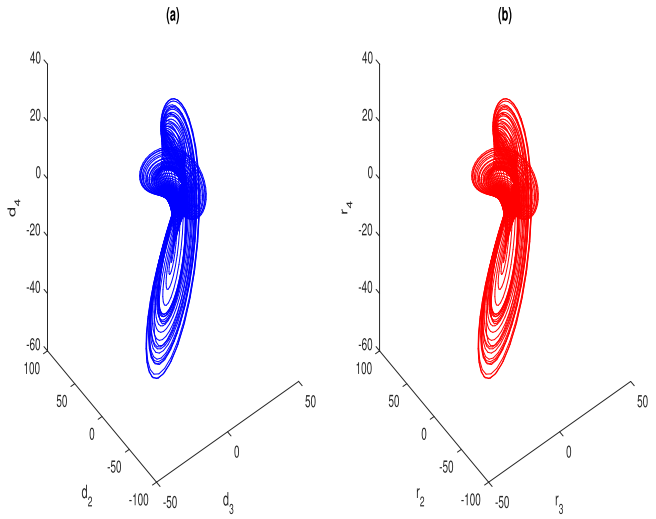

Figure 10. Chaotic solutions for (a) the integer-order drive model (2.0.2) in (d_3, d_2, d_4) space and (b) the two FO response models (5.1.1)–(5.1.2) in (r_3, r_2, r_4).

For the choice $M_1 = \begin{pmatrix} 1 & 0 & 0 \\ 0 & 1 & -1 \\ 1 & 0 & 1 \\ 0 & -1 & 2 \\ 0 & 0 & 1 \end{pmatrix}$, $M_2 = M_3 = I_{5\times5}$, where $I_{5\times5}$ is (5×5) identity matrix, and $K = diag(1, 2, 3, 4, 5)$, the vector function $\tau(u, v, w)$ can be obtained from theorem 5.1 as:

$$\tau(u,\ v,\ w) = \begin{pmatrix} u_3u_5 - v_2v_3 - w_3w_5 - a - e_1 \\ u_4u_5 - v_1^2 + v_2 - 4v_1 - w_4w_5 + 1 - 2e_2 \\ u_1^2 - u_2^2 - u_3 - v_2v_3 + 4v_1 - w_1^2 + w_2^2 + w_3 - a - 1 - 3e_3 \\ 2u_1u_2 - u_4 + v_1^2 - v_2 + 8v_1 - 2w_1w_2 + w_4 - 2 - 4e_4 \\ -4u_1 + 4v_1 + 4w_1 - 1 - 5e_5 \end{pmatrix}, \tag{5.1.3}$$

where $e_1 \equiv r_1 - d_1 = (v_1 + w_1) - u_1$, $e_2 \equiv r_2 - d_2 = (v_2 - v_3 + w_2) - u_2$, $e_3 \equiv r_3 - d_3 = (v_1 + v_3 + w_3) - u_3$, $e_4 \equiv r_4 - d_4 = (-v_2 + 2v_3 + w_4) - u_4$ and $e_5 \equiv r_5 - d_5 = (v_3 + w_5) - u_5$.

In numerical simulation, we used Runge-Kutta method of order 4 and PECE (PredictorEvoluteCorrectorEvolute) method [41]. If we take $a = 0.075$, $q = 0.995$ and the initial conditions of the integer-order drive model (2.0.2) and the two FO response models (5.1.1)–(5.1.2) are, respectively, $u_0 = (2{,}1,\ 3{,}2{,}9)^T$, $v_0 = (1{,}2{,}2)^T$ and $w_0 = (1.1,\ 1.2,\ -0.3,\ 2.2,\ 6.5)^T$ as an example. The results of CS of our models are given in figures 10–11. Figure 10 shows the projection (3D) of the solution of the integer-order drive model (2.0.2) and the two FO response models (5.1.1)–(5.1.2) after synchronization. The synchronization errors converge zero as depicted in figure 11.

6. Conclusion and future work

Models (2.0.2), (3.0.1) and (4.0.1) with chaotic and hyperchaotic hidden attractors are introduced which have rich dynamics. These models have only one stable equilibrium. Firstly, we proposed the hyperchaotic complex integer model (2.0.2). This model has 2, 4, 6, and 10 scrolls hidden attractors for a small change in the parameter a, as shown in figure 2. According to computed LEs, our model, (2.0.2), exhibits hyperchaotic MSHAs while the integer version, (1.0.1), does not (see figure 4). Secondly, model (3.0.1) is presented which is the fractional version of model (1.0.1). The security provided by this model is more complicated than that provided by the integer one (1.0.1) due to the availability of the fractional parameter q. Furthermore, the basic properties of this model are investigated using phase diagrams, bifurcation diagrams, and LEs, as shown in figure 4. Finally, the FO complex model (4.0.1) is given. It is found that this model has one stable equilibrium point and is very sensitive to its model parameters a $(a > 0)$ and q. We provide our findings for MSHAs of this model in figures 7–9. As illustrated in figures 1 and figure 6(b), the parameter a interval at which model (4.0.1) contains chaotic MSHAs is bigger than the one for model (2.0.2). The MSHAs exist only for the complex integer-order model (2.0.2) and the complex FO model (4.0.1). We introduce the CS between one integer-order drive model and two FO response

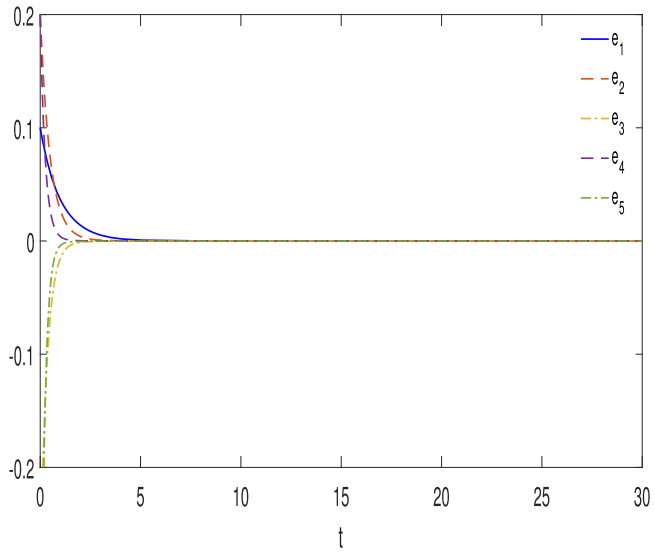

Figure 11. Synchronization errors for the integer-order drive model (2.0.2) and the two FO response models (5.1.1)–(5.1.2).

models with different dimensions as a new kind of synchronization. The tracking control method is used to present a scheme of this kind of synchronization. As an example of our technique, we present the CS between the integer-order drive model (2.0.2) and the two FO response models (5.1.1)–(5.1.2). The numerical results of CS of our models are shown in figures 10–11 and a good agreement is found with the analytical ones. These models may have applications in physics, image encryption and secure communication.

We are currently working to expand these findings to include time delay for our systems (2.0.2), (3.0.1) and (4.0.1).

Data availability statement

All data that support the findings of this study are included within the article (and any supplementary files).

Conflict of interest

The authors declare that they have no conflict of interest.

ORCID iDs

Tarek M Abed-Elhameed https://orcid.org/0000-0002-8816-6376

References

[1] Suykens J and Chua L 1997 n-double scroll hypercubes in 1-D CNNs *Int. J. Bifurcation Chaos* **7** 1873–85
[2] Yin Q and Wang C 2018 A new chaotic image encryption scheme using breadth-first search and dynamic diffusion *Int. J. Bifurcation Chaos* **28** 1850047
[3] Mahmoud G M, Farghaly A A, Abed-Elhameed T M and Darwish M M 2018 Adaptive dual synchronization of chaotic (hyperchaotic) complex systems with uncertain parameters and its application in image encryption *Acta Phys. Pol.* B **49** 1923
[4] Li K-Z, Zhao M-C and Fu X-C 2009 Projective synchronization of driving-response systems and its application to secure communication *IEEE Transactions on Circuits and Systems I: Regular Papers* **56** 2280–91
[5] Sieber J and Krauskopf B 2008 Control based bifurcation analysis for experiments *Nonlinear Dyn.* **51** 365–77
[6] Mahmoud G M, Bountis T, AbdEl-Latif G and Mahmoud E E 2009 Chaos synchronization of two different chaotic complex Chen and Lü systems *Nonlinear Dyn.* **55** 43–53
[7] Mahmoud G M, Bountis T and Mahmoud E E 2007 Active control and global synchronization of the complex Chen and Lü systems *Int. J. Bifurcation Chaos* **17** 4295–308
[8] Mahmoud G M, Ahmed M E and Abed-Elhameed T M 2016 Active control technique of fractional-order chaotic complex systems *The European Physical Journal Plus* **131** 200
[9] Mahmoud G M, Ahmed M E and Abed-Elhameed T M 2017 On fractional-order hyperchaotic complex systems and their generalized function projective combination synchronization *Optik* **130** 398–406
[10] Shilnikov L P 1965 A case of the existence of a denumerable set of periodic motions *Doklady Akademii Nauk* vol 160 (Russian Academy of Sciences) pp 558–61

[11] Leonov G A and Kuznetsov N V 2013 Hidden attractors in dynamical systems. From hidden oscillations in Hilbert-Kolmogorov, Aizerman, and Kalman problems to hidden chaotic attractor in Chua circuits *Int. J. Bifurcation Chaos* **23** 1330002
[12] Leonov G, Kuznetsov N and Mokaev T 2015 Homoclinic orbits, and self-excited and hidden attractors in a Lorenz-like system describing convective fluid motion *The European Physical Journal Special Topics* **224** 1421–58
[13] Wang X, Kuznetsov N V and Chen G 2021 *Chaotic Systems with Multistability and Hidden Attractors* (Springer)
[14] Wang X and Chen G 2012 A chaotic system with only one stable equilibrium *Commun. Nonlinear Sci. Numer. Simul.* **17** 1264–72
[15] Sprott J C 1994 Some simple chaotic flows *Phys. Rev.* E **50** R647–50
[16] Huang L and Bae Y 2018 Chaotic dynamics of the fractional-love model with an external environment *Entropy* **20** 53
[17] Huang L and Bae Y 2019 Nonlinear behavior in fractional-order Romeo and Juliet's love model influenced by external force with fuzzy function *Int. J. Fuzzy Syst.* **21** 630–8
[18] Khan N A, Qureshi M A, Akbar S and Ara A 2022 From chaos to encryption using fractional order Lorenz-Stenflo model with flux-controlled feedback memristor *Phys. Scr.* **98** 014002
[19] Shen Y, Zou T, Zhang L, Wu Z, Su Y and Yan F 2022 A novel solar radio spectrogram encryption algorithm based on parameter variable chaotic systems and dna dynamic encoding *Phys. Scr.* **97** 055210
[20] Khan N A, Qureshi M A, Hameed T, Akbar S and Ullah S 2020 Behavioral effects of a four-wing attractor with circuit realization: a cryptographic perspective on immersion *Commun. Theor. Phys.* **72** 125004
[21] Ramakrishnan B, Welba C, Chamgoué A C, Karthikeyan A and Kingni S T 2022 Autonomous jerk oscillator with sine nonlinearity and logistic map for sEMG encryption *Phys. Scr.* **97** 095211
[22] Chen Y, Xie S and Zhang J 2022 A novel double image encryption algorithm based on coupled chaotic system *Phys. Scr.* **97** 065207
[23] Khan N A, Hameed T, Qureshi M A, Akbar S and Alzahrani A K 2020 Emulate the chaotic flows of fractional jerk system to scramble the sound and image memo with circuit execution *Phys. Scr.* **95** 065217
[24] Deng Q and Wang C 2019 Multi-scroll hidden attractors with two stable equilibrium points *Chaos* **29** 093112
[25] Wang N, Li C, Bao H, Chen M and Bao B 2019 Generating multi-scroll Chua's attractors via simplified piecewise-linear Chua's diode *IEEE Transactions on Circuits and Systems I: Regular Papers* **66** 4767–79
[26] Suykens J A and Vandewalle J 1993 Generation of n-double scrolls (n=1, 2, 3, 4,…) *IEEE Transactions on Circuits and Systems I: Fundamental Theory and Applications* **40** 861–7
[27] Wu Q, Hong Q, Liu X, Wang X and Zeng Z 2020 A novel amplitude control method for constructing nested hidden multi-butterfly and multiscroll chaotic attractors *Chaos, Solitons Fractals* **134** 109727
[28] Wu Y, Wang C and Deng Q 2021 A new 3D multi-scroll chaotic system generated with three types of hidden attractors *The European Physical Journal Special Topics* **230** 1863–71
[29] Liu S, Wei Y, Liu J, Chen S and Zhang G 2020 Multi-scroll chaotic system model and its cryptographic application *Int. J. Bifurcation Chaos* **30** 2050186
[30] Wang F and Xiao Y 2020 A multiscroll chaotic attractors with arrangement of saddle-shapes and its field programmable gate array (FPGA) implementation *Complexity* **2020** 9169242
[31] Li-Quan X, Shu-Kai D and Li-Dan W 2018 Julia fractal based multi-scroll memristive chaotic system *Acta Phys. Sin.* **67** 090502
[32] Khan A, Jahanzaib L S, Khan T and Trikha P 2020 Secure communication: using fractional matrix projective combination synchronization *AIP Conference Proceedings* vol 2253 (AIP Publishing LLC) 020009
[33] Zerimeche H, Houmor T and Berkane A 2021 Combination synchronization of different dimensions fractional-order non-autonomous chaotic systems using scaling matrix *International Journal of Dynamics and Control* **9** 788–96
[34] Mahmoud G, Khalaf H, Darwish M and Abed-Elhameed T 2022 Different kinds of modulus-modulus synchronization for chaotic complex systems and their applications *Acta Phys. Pol.* B **53** A2.1–A2.28
[35] Yan S, Wang Q, Wang E, Sun X and Song Z 2022 Multi-scroll fractional-order chaotic system and finite-time synchronization *Phys. Scr.* **97** 025203
[36] Benettin G, Galgani L, Giorgilli A and Strelcyn J-M 1980 Lyapunov characteristic exponents for smooth dynamical systems and for Hamiltonian systems; a method for computing all of them. Part 1: Theory *Meccanica* **15** 9–20
[37] Benettin G, Galgani L and Strelcyn J-M 1976 Kolmogorov entropy and numerical experiments *Phys. Rev.* A **14** 2338
[38] Wolf A, Swift J B, Swinney H L and Vastano J A 1985 Determining Lyapunov exponents from a time series *Physica D* **16** 285–317
[39] Frederickson P, Kaplan J L, Yorke E D and Yorke J A 1983 The Liapunov dimension of strange attractors *J. Differ. Equ.* **49** 185–207
[40] Caputo M 1967 Linear models of dissipation whose Q is almost frequency independentII *Geophys. J. Int.* **13** 529–39
[41] Diethelm K, Ford N J and Freed A D 2002 A predictor-corrector approach for the numerical solution of fractional differential equations *Nonlinear Dyn.* **29** 3–22
[42] Yang L x, He W s and Liu X j 2011 Synchronization between a fractional-order system and an integer order system *Computers and Mathematics with Applications* **62** 4708–16
[43] Runzi L, Yinglan W and Shucheng D 2011 Combination synchronization of three classic chaotic systems using active backstepping design *Chaos* **21** 043114
[44] Sun J, Cui G, Wang Y and Shen Y 2015 Combination complex synchronization of three chaotic complex systems *Nonlinear Dyn.* **79** 953–65
[45] Mahmoud G M, Abed-Elhameed T M and Khalaf H 2021 Synchronization of hyperchaotic dynamical systems with different dimensions *Phys. Scr.* **96** 125244
[46] Yang L-x, He W-s and Liu X-j 2011 Synchronization between a fractional-order system and an integer order system *Comput. Math. Appl.* **62** 4708–16
[47] Aguila-Camacho N, Duarte-Mermoud M A and Gallegos J A 2014 Lyapunov functions for fractional order systems *Commun. Nonlinear Sci. Numer. Simul.* **19** 2951–7